Radial Density Distribution of Chromatin: Evidence that Chromatin Fibers Have Solid Centers

Michael F. Smith, Brian D. Athey, Shawn P. Williams, and John P. Langmore

Biophysics Research Division and Department of Biological Sciences, The University of Michigan, Ann Arbor, Michigan 48109

Abstract. Fiber diameter, radial distribution of density, and radius of gyration were determined from scanning transmission electron microscopy (STEM) of unstained, frozen-dried chromatin fibers. Chromatin fibers isolated under physiological conditions (ionic strength, 124 mM) from *Thyone briareus* sperm (DNA linker length, n = 87 bp) and *Necturus maculosus* erythrocytes (n = 48 bp) were analyzed by objective image-processing techniques. The mean outer diameters were determined to be 38.0 nm (SD = 3.7 nm; SEM = 0.36 nm) and 31.2 nm (SD = 3.6 nm; SEM = 0.32 nm) for *Thyone* and *Necturus*, respectively. These data are inconsistent with the twisted-ribbon and solenoid models, which predict constant diameters of ~30 nm, independent of DNA linker length. Calculated radial density distributions of chromatin exhibited relatively uniform density with no central hole, although the 4-nm hole in tobacco mosaic virus (TMV) from the same micrographs was visualized clearly. The existence of density at the center of chromatin fibers is in strong disagreement with the hollow-solenoid and hollow-twisted-ribbon models, which predict central holes of 16 and 9 nm for chromatin of 38 and 31 nm diameter, respectively. The cross-sectional radii of gyration were calculated from the radial density distributions and found to be 13.6 nm for *Thyone* and 11.1 nm for *Necturus*, in good agreement with x-ray and neutron scattering. The STEM data do not support the solenoid or twisted-ribbon models for chromatin fiber structure. They do, however, support the double-helical crossed-linker models, which exhibit a strong dependence of fiber diameter upon DNA linker length and have linker DNA at the center.

ELUCIDATION of the three-dimensional structure of the condensed chromatin fiber will be an important step in the understanding of the mechanism of eukaryotic gene expression. The highly conserved structural subunit of chromatin is the nucleosome core particle. It is composed of 146 bp of DNA wrapped around the globular histone octamer, with a height of 5.7 nm and a diameter of 11.0 nm (22). The nucleosome cores are connected by a tissue-specific amount of linker DNA ranging from 20 to 100 bp. There is strong evidence that the tissue-specific histone, H1, binds within this variable linker region (1). Packaging of these conserved and variable components elicit the formation of the condensed "30 nm" chromatin fiber observed under physiological conditions (for review see references 10, 32, 33).

Chromatin fiber structure has been studied by a variety of techniques including EM (6, 11, 13, 17, 29, 30, 35, 37–40), x-ray scattering (3, 4, 14, 15, 17, 34–37), neutron scattering (2, 9, 13, 28), dichroism and rotational relaxation measurements (7, 14, 20, 23), and sedimentation velocity measurements (5, 31). Divergent results and different interpretations of similar results have led to the proposal of three classes of helical models for the condensed chromatin fiber: the solenoid, the twisted-ribbon, and the crossed-linker models. Predicted side and end-on views of these structures are illustrated in Figs. 1, 2, and 3.

The solenoid model, outlined by Finch and Klug (11), is a single-start "contact helix" with five to seven nucleosomes per turn and has a diameter of ~30 nm, a 10-nm central hole, and linker DNA closely associated with the nucleosome core. Elaborating on this model, McGhee et al. (20) proposed a superhelical path for the linker DNA between adjacent nucleosomes (Fig. 1, *a* and *b*). In these hollow-solenoid models, different DNA linker lengths result in different nucleosome orientations and interactions. Alternatively, Butler (5) proposed the solid-solenoid model in which the linker DNA is looped into the center of the fiber, conserving interactions among nucleosomes. Solenoid models predict a helical pitch of 11 nm (the diameter of a nucleosome) and a diameter that should depend upon the number of nucleosomes per helical turn, although the number has been historically assumed to be five to seven.

The twisted-ribbon model was originally proposed by Worcel et al. (39), and further discussed by Woodcock et al. (38). They were motivated by the zigzag pattern of nucleosomes observed by EM of chromatin at low ionic strength (30, 38, 39). The Worcel model describes two parallel columns (the ribbon) of stacked nucleosomes connected by linker DNA, which are twisted in a superhelix around a central axis. This structure has a pitch that is dependent upon DNA linker length, a solid nucleoprotein center, conserved

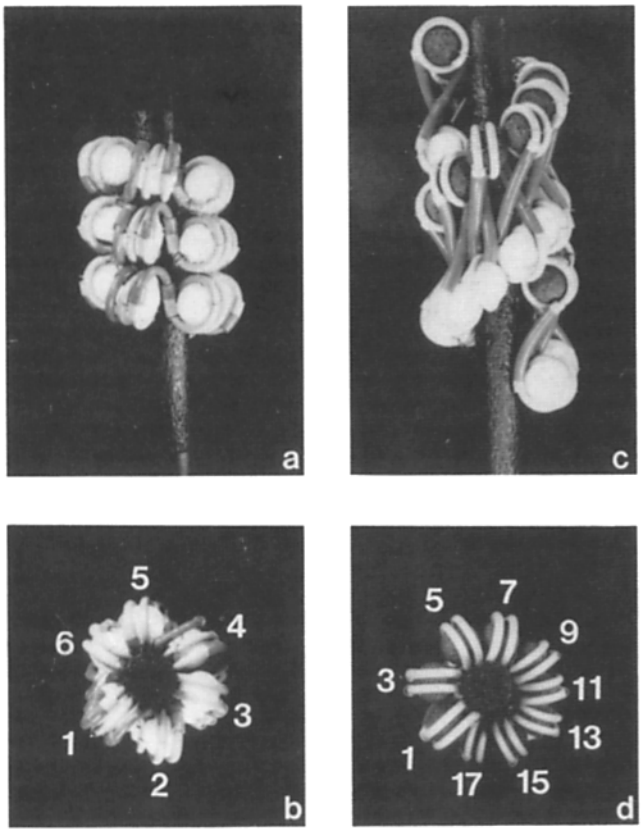

Figure 1. Space-filling models illustrating two major classes of structures proposed for chromatin. Core DNA is shown in grey; linker DNA (n = 48 bp, as in *Necturus* erythrocytes) is shown in black. Numbers indicate the sequence of nucleosomes. (*a* and *b*) Side and end-on views of the hollow-solenoid model. The model has a helical repeat of six nucleosomes per 11 nm; pitch of 11 nm; diameter of 30 nm; and central hole of 8.0 nm diameter. (*c* and *d*) Side and end-on views of the twisted-ribbon model, showing the single ribbon of dinucleosomes consisting of the even (white) and odd (black) nucleosome cores. The model has a helical repeat of 18 nucleosomes per 32 nm; pitch of 32 nm; diameter of 30 nm; and central hole of 8.0 nm diameter.

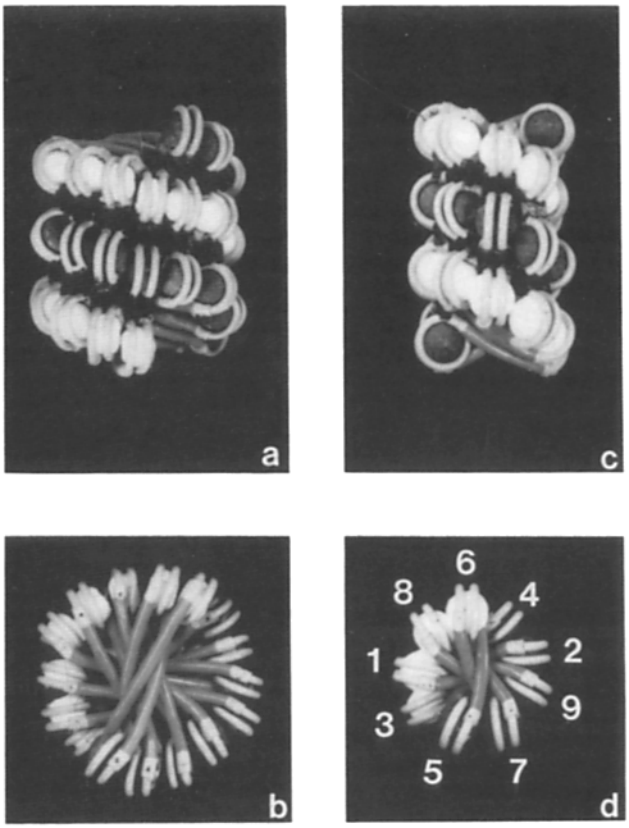

Figure 2. Space-filling models illustrating the double-helical crossed-linker model. Core DNA is shown in grey; linker DNA in black; odd nucleosomes are represented with black cores; and even nucleosomes with white cores. Numbers indicate the sequence of nucleosomes. (*a* and *b*) Side and end-on views of a double-helical crossed-linker model formed from a $\Delta L = -2$ ribbon with *Thyone* sperm DNA linker length (n = 87 bp). This model has a helical repeat of 12 nucleosomes per 13 nm; pitch of 26 nm; diameter of 45 nm; and no central hole. (*c* and *d*) Side and end-on views of a double-helical crossed-linker model formed from a $\Delta L = -2$ ribbon with *Necturus* erythrocyte DNA linker length (n = 48 bp). This model has a helical repeat of nine nucleosomes per 13 nm; pitch of 26 nm; diameter of 31 nm; and no central hole.

interactions among nucleosomes, and a diameter that depends very slightly upon DNA linker length. The Woodcock model (Fig. 1 *c*) describes a twisted ribbon in which the linker DNA zigzags up and down almost parallel to the fiber axis. This structure has a pitch that is dependent upon DNA linker length, a hollow center (Fig. 1 *d*), conserved interactions among nucleosomes, and a conserved diameter.

Williams et al. (37) proposed a double-helical crossed-linker model for chromatin in which the linker DNA crosses the fiber axis, placing successive nucleosomes on opposite sides of the helical axis. Other crossed-linker models have been proposed (4, 19, 24), the major differences being the path of the linker DNA, the number of helical gyres, and the radial distribution of density. Figs. 2 and 3 illustrate the predicted side and end-on views of the double-helical crossed-linker model proposed by Williams et al. This model has a DNA-filled center, a pitch of 26–27 nm, conserved interactions among nucleosomes, and a diameter that depends strongly upon DNA linker length but not the number of nucleosomes per turn.

The double-helical crossed-linker models have two structural characteristics that distinguish them from the solenoid and twisted-ribbon models: (*a*) strong fiber diameter dependence upon DNA linker length; and (*b*) high-density at the center of the fibers. These differences are distinguishable using the technique of scanning transmission electron microscopy (STEM) in conjunction with computer image processing. Previous STEM studies of tobacco mosaic virus (TMV) and TMV coat protein (26), the tail-tube of bacteriophage T4 (8), and the fimbriae of *Bordetella pertussis* (25) have established the sensitivity of STEM to distinguish between hollow and solid centers of fibrous biological molecules.

We describe the quantitative analysis of dark field STEM images to determine the fiber diameters, radial density distributions, and radii of gyration of chromatin fibers from *Thyone* sperm and *Necturus* erythrocytes. The results indicate: (*a*) a larger diameter for fibers with greater DNA linker length; and (*b*) a relatively uniform distribution of density through-

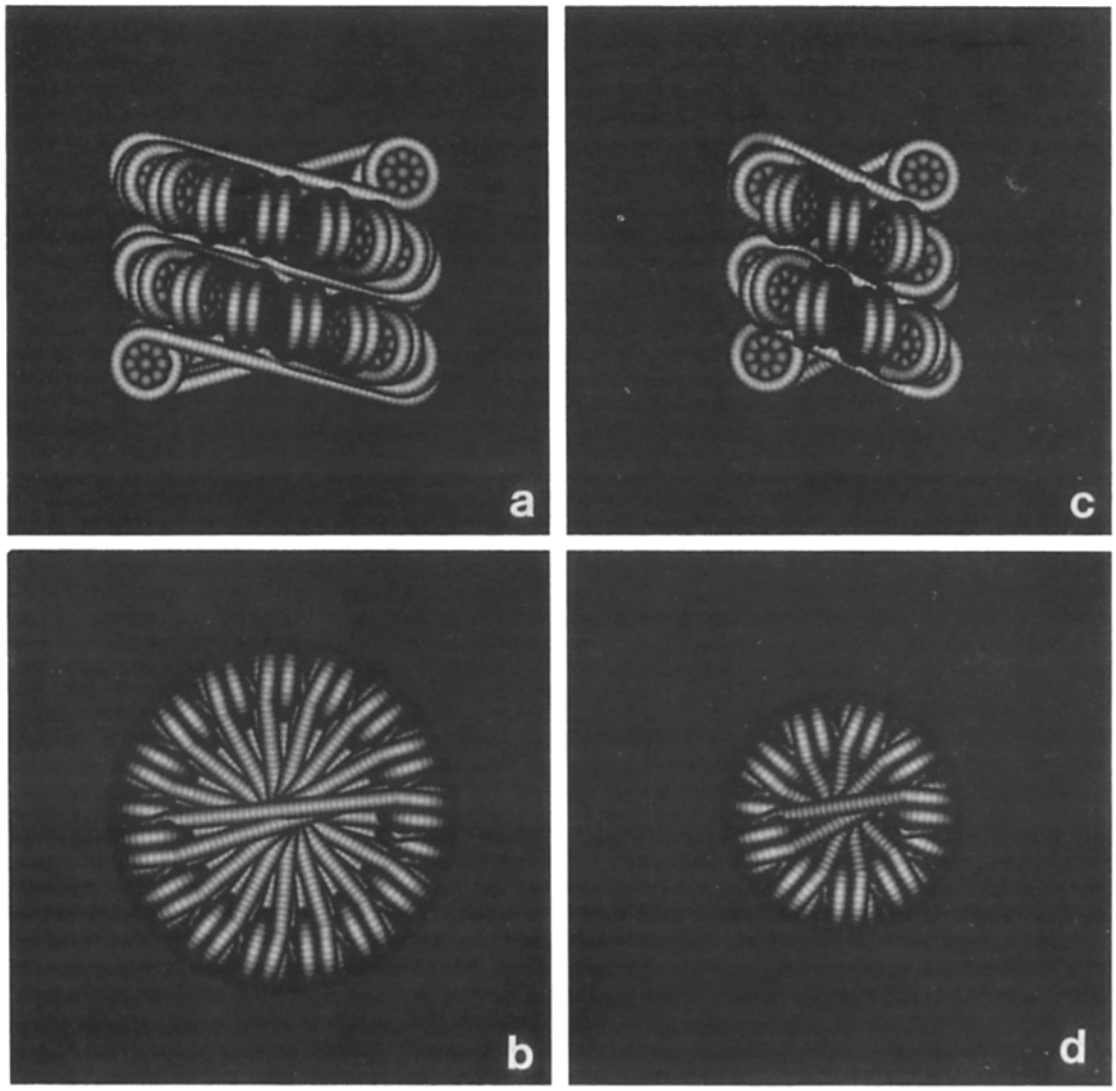

Figure 3. Computer-generated crossed-linker models. (*a* and *b*) Side and end-on views of a double-helical crossed-linker model (n = 87 bp) formed from a $\Delta L = -2$ ribbon. This model has a helical repeat of 16 nucleosomes per 13.5 nm; pitch of 27 nm; diameter of 41.9 nm (measured at 15% maximum mass thickness); and no central hole. (*c* and *d*) Side and end-on views of a double-helical crossed-linker model (n = 49 bp) formed from a $\Delta L = -2$ ribbon. This model has a helical repeat of 10 nucleosomes per 13 nm; pitch of 26 nm; diameter of 28.3 nm (measured at 15% maximum mass thickness); and no central hole.

out the fibers with no evidence of a central hole. Together, these data are inconsistent with the proposed solenoid and twisted-ribbon models. These data are most compatible with the double-helical crossed-linker models.

Materials and Methods

Specimens

Thyone briareus (sea cucumber) sperm chromatin, and *Necturus maculosus* (mudpuppy) erythrocyte chromatin were isolated at physiological conditions (ionic strength, 124 mM) as previously described (37). DNA linker lengths were calculated by subtracting 146 bp from the published nucleosomal DNA repeat lengths (37).

Electron Microscopy

STEM images were recorded at the Brookhaven National Laboratory. Chromatin samples were fixed in buffer EB (60 mM KCl, 15 mM NaCl, 15 mM Pipes pH 7.0, 3.0 mM EDTA, and 0.02% NaN_3) with 0.5% glutaraldehyde for 1–3 d at 0°C and injected into a drop of 100 mM ammonium acetate on a fresh carbon film. After 2–4 min, the samples were washed with 12 drops of 100 mM ammonium acetate and freeze-dried overnight. Samples were examined at −160°C with the 40 keV electron beam focused to 0.25 nm. 512 × 512 pixel images were recorded at a sampling interval (pixel size) of 2.0 nm and a radiation dose of 100–300 e^-/nm^2. As a control for radiation dose effects, a few images were recorded with a pixel size of 1.0 nm at a dose of 400–1,200 e^-/nm^2. The outer annular detector dark field signals were converted to scattering probabilities, which are proportional to mass thickness (mass per unit area) (16).

Computer Modeling

Nucleosome cores were created from a combination of "protein" and "DNA" ellipsoids that gave calculated x-ray scattering curves best approximating the observed x-ray scattering of the core particles in solution 35. The octamer core was modeled as 18 spheres of 1.1 nm diameter. Core DNA was built from 59 overlapping spheres of 1.9 nm diameter, representing 1.75 left-handed turns of DNA, centered at a radius of 42.5 nm and having a pitch of 2.7 nm. Electron scattering densities were calculated from the elemental

composition of an average protein and sodium DNA molecule for 40 keV electrons (18) and the calculated collection efficiencies for the outer annular detector of the Brookhaven STEM, which subtends 40–200 mrad. Total scattering was based on the known molecular weight of the histone octamer and nucleosomal DNA. Histone H1 was not included due to uncertainty in its position.

The hollow-solenoid models were generated according to the description of McGhee et al. (20) with the linker DNA following a continuous superhelical path. The left-handed double-helical crossed-linker models were generated according to the $\Delta L = -2$ pattern described by Williams et al. (37) with the linker DNA following a straight path between nucleosomes. The *Thyone* crossed-linker model had only one close DNA-DNA interaction, having a center-to-center distance of 1.6 nm. This close contact occurred ~0.9 nm from the chromatin axis. The *Necturus* crossed-linker model had no DNA center-to-center distances of less than 1.9 nm. For both models, no other contacts between DNA molecules were closer than 2.7 nm. The crossed-linker models were built with DNA linker lengths of 24.5 and 17.3 nm to best fit the STEM measurements of outer diameter. For all models, the relative amounts of scattering from linker DNA and the nucleosome core was based on the published DNA linker lengths. Modeling will be described more fully in a later paper.

Image Processing

Image processing was performed using interactive software (EMPRO programs, written in FORTRAN) on a Silicon Graphics IRIS 2500T workstation. The radial density distribution programs (TOTAL and PROFILE) described by Steven et al. (26, 27) were integrated into the software.

Chromatin fibers were chosen for analysis based on the qualitative criteria of straightness, uniformity of diameter, lack of observable aggregation, and low residual salt background. About 10% of the fibers met this criteria. Typical fiber segments were 40–50 nm long and no closer than 10 nm from the ends of the fibers.

The first steps in the analysis were: (*a*) projection of the mass thickness of individual fiber segments down the long axis; (*b*) calculation of fiber diameter from the projections; and (*c*) addition of the projections of independent groups of fibers. The orientation of each fiber axis was estimated using the interactive graphics and digitally refined by cross-correlation methods (27). Mass thicknesses were projected down the refined axis into "bins" representing one-third or one-half the pixel dimension, using the technique of "Vernier sampling" (26, 27). Two estimates of the fiber diameter were numerically determined from each projection: (*a*) the distance between the points that were 50% of the maximum mass thickness (referred to as the full width at half maximum); and (*b*) the distance between the points that were 15% of the maximum mass thickness (referred to as the outer diameter). On average, 98% of the experimental fiber mass was within this outer diameter. After the calculation of diameter, projections that upon visual inspection exhibited obvious deviations from mirror symmetry were discarded, leaving 70% of the originally chosen chromatin fibers. The remaining projections were divided into groups depending upon outer diameter, pixel size, and bin size. The projections from within each group were aligned and combined using cross-correlation methods. Each combined projection represented an independent average of fiber segments that had met the previously stated criteria, and contained 10–25 independent projections (a combined length of 0.5–1.2 μm of chromatin).

The cylindrically averaged projections of the computer-generated models were intentionally smeared to generate a projection that was directly comparable to the STEM data. Smearing was performed by convolution of the model projections with a smoothed and truncated Gaussian function. A Gaussian function with the same SD as the STEM diameter data (σ = 3.7 nm) was truncated at $\pm \sigma$, and subsequently smoothed by convolution with a second Gaussian function. The second function had a SD equal to that of the grouped projections used for the radial density calculations (σ = 1.6 nm). The smeared projections were normalized for display assuming that histone H1, which was not included in the computer-generated models, represents 10% of the total mass. Thus, the area under the model projections was equal to 90% of the area under the empirical mass thickness projections.

The final steps in the analysis were: (*a*) calculation of the radial mass densities from the combined projections; and (*b*) calculation of the cross-sectional radii of gyration from the radial density distributions. Radial densities were calculated using a real-space algorithm applicable to cylindrically symmetric molecules and averages of helically symmetric molecules randomly-oriented about their long axis (26, 27). Although all fiber projections were included in the calculation of the fiber diameter, only those projections that gave outer diameters within one SD of the mean were used in the radial density calculations. Standard errors were calculated from six individual density distributions derived from independent groups of projections that were grouped according to outer diameter. Radial density distributions obtained from the projections of the computer-generated models were normalized to 90% total mass, as described for the mass thickness projections. The cross-sectional radii of gyration were calculated from the experimental and theoretical radial density distributions.

Results

Diameter Measurements

TMV, *Thyone*, and *Necturus* fibers were analyzed for outer diameter. STEM images representative of the micrographs that were analyzed are given in Fig. 4. Histograms of the computer-measured outer diameters (Fig. 5) demonstrate the

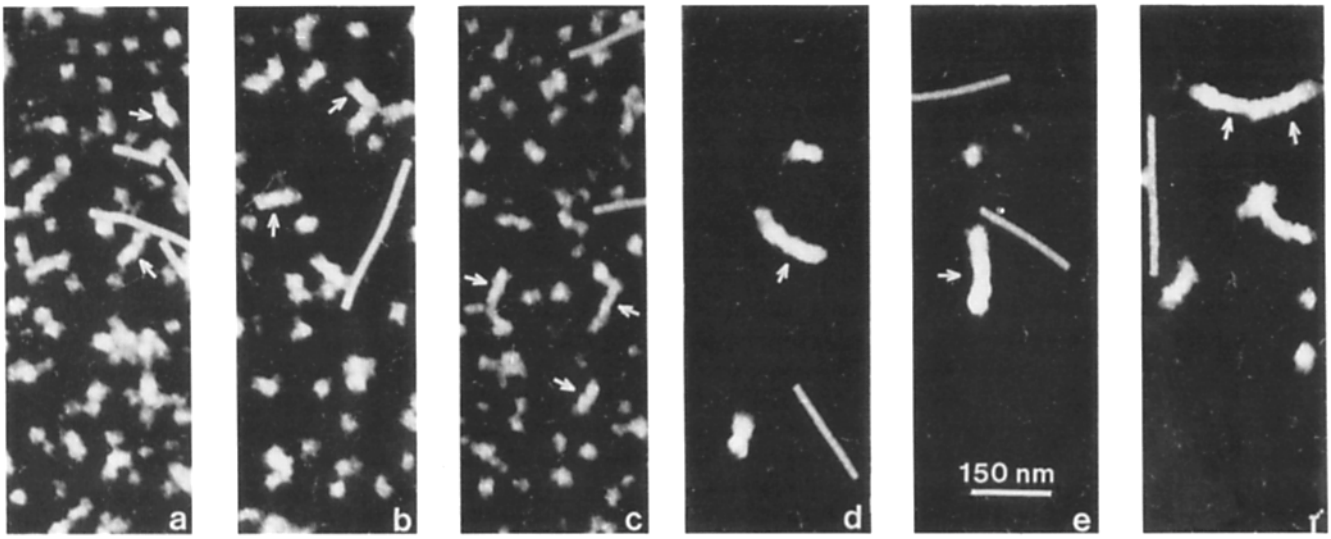

Figure 4. STEM images of unstained chromatin fibers from *Necturus* erythrocytes (*a*, *b*, and *c*) and *Thyone* sperm (*d*, *e*, and *f*). Arrows indicate fiber segments representative of those chosen for analysis. The thin, rod-like structures seen in the STEM images are the TMV particles used as an internal control.

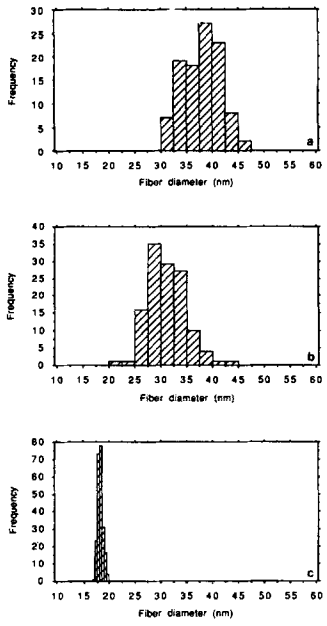

Figure 5. Histograms of fiber outer diameters determined from mass thickness projections. (*a*) *Thyone* sperm chromatin (mean diameter, 38.0 nm; SD, 3.7 nm; SEM, 0.36 nm; number of measurements, 104). (*b*) *Necturus* erythrocyte chromatin (mean diameter, 31.2 nm; SD, 3.6 nm; SEM, 0.32 nm; number of measurements, 125). (*c*) TMV (mean diameter, 18.1 nm; SD, 0.6 nm; SEM, 0.04 nm; number of measurements, 226).

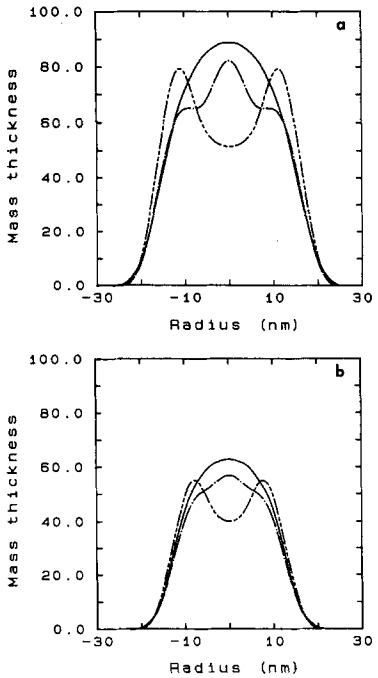

Figure 7. (*a*) Mass thickness projections of *Thyone* chromatin and corresponding computer-generated models. (———) Average mass thickness projection of *Thyone* sperm chromatin. The projection was obtained by combining 28 fiber segments corresponding to a cumulative length of ~1.2 μm of chromatin, and had an outer diameter of 38.3 nm (measured at 15% maximum mass thickness). (— · —) Smoothed projection of a cylindrically-averaged double-helical crossed-linker model. (– – – –) Smoothed projection of a cylindrically-averaged hollow-solenoid model. Both models had outer diameters of 38.5 nm. The ordinate is not scaled to represent absolute mass thickness. (*b*) Mass thickness projections of *Necturus* chromatin and corresponding computer-generated models. (———) Average mass thickness projection of *Necturus* erythrocyte chromatin. The projection was obtained by combining 36 fiber segments corresponding to a cumulative length of ~1.6 μm of chromatin, and had a measured outer diameter of 31.4 nm (measured at 15% maximum mass thickness). (— · —) Smoothed projection of a cylindrically-averaged double-helical crossed-linker model. (– – – –) Smoothed projection of a cylindrically averaged hollow-solenoid model. Both models had outer diameters of 31.6 nm. The ordinate is not scaled to represent absolute mass thickness.

difference between the *Thyone* and *Necturus* diameter distributions. The mean outer diameters were 38.0 nm (SD = 3.7 nm; SEM = 0.36 nm) and 31.2 nm (SD = 3.6 nm; SEM = 0.32 nm), respectively. The low standard errors (<1%), in addition to the results of a *t* test ($P < 0.0001$), provided strong evidence that the two populations had significantly different diameters. Full width at half maximum diameters (less sensitive to background noise) were calculated as a control, and gave values of 29.0 nm (SD = 2.2; SEM = 0.21 nm) for *Thyone* and 24.8 nm (SD = 2.4 nm; SEM = 0.21) for *Necturus*. Hence, the ratio of *Thyone* to *Necturus* diameters did not depend upon the method of choosing the fiber edge. The mean outer and full width at half maximum diameters found for TMV were 18.1 nm (SD = 0.6 nm; SEM = 0.04 nm) and 15.0 nm (SD = 0.5 nm; SEM = 0.03 nm), respectively. That the SD of the TMV diameters was much less than that of chromatin indicates that chromatin is a more heterogeneous structure than TMV.

Radial Distribution of Density

The calculation of radial density provides information relating to the distribution of density within a fiber. These distributions were compared with those from known structures and to those predicted from proposed models. TMV was used as a control owing to its known structure and known radial density distribution. Our radial reconstruction of TMV is illustrated in Fig. 6. This distribution exhibits three internal density peaks at approximate radii of 2.7, 5.0, and 6.8 nm. A central depression in density of 1–2 nm in radius is also observed.

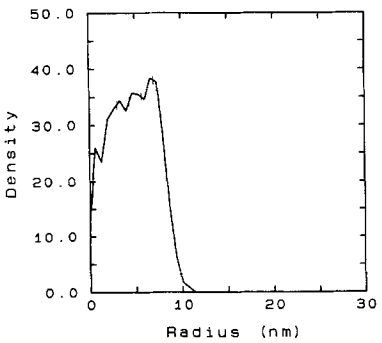

Figure 6. Radial density distribution of TMV calculated from dark-field STEM images. The averaged projection contained 46 fiber segments, corresponding to ~1.5 μm of TMV. Error bars represent the SEM (mean error, 0.8 nm), calculated from 10 individual radial density profiles (each an average of 23 segments). The ordinate is not scaled to represent absolute density.

Averaged mass thickness projections of *Thyone* sperm chromatin and *Necturus* erythrocyte chromatin are given in Fig. 7. Projections of computer-generated densities predicted by the crossed-linker and hollow-solenoid models also are shown for comparison. Clearly the data are inconsistent with the projections of the hollow-solenoid models.

Radial density distributions that correspond to the above projections are illustrated in Fig. 8. The empirically deter-

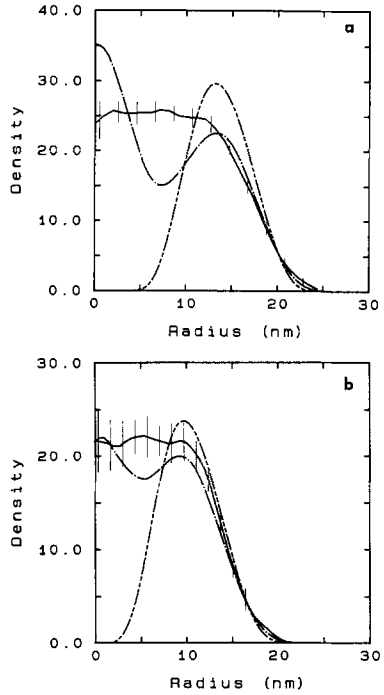

Figure 8. (*a*) Radial density distributions of (———) *Thyone* sperm chromatin, (— · —) the crossed-linker model, and (– – – –) the hollow-solenoid model, derived from the mass thickness projections given in Fig. 7 *a*. Error bars represent the SEM (mean error, 1.0 nm), calculated from six individual radial density distributions (each an average of seven segments). The ordinate is not scaled to represent absolute density. (*b*) Radial density distributions of (———) *Necturus* erythrocyte chromatin, (— · —) the crossed-linker model, and (– – – –) the hollow-solenoid model, derived from the mass thickness projections given in Fig. 7 *b*. Error bars represent the SEM (mean error, 1.9 nm), calculated from six individual radial density distributions (each an average of nine segments). The ordinate is not scaled to represent absolute density.

mined *Thyone* and *Necturus* chromatin distributions exhibit relatively uniform density at all radii, with no evidence of a central hole. The radial density distributions of the crossed-linker models also exhibit high density at all radii. The theoretical *Necturus* distribution agrees well with the data, with most of the distribution falling within the calculated experimental error. The theoretical *Thyone* distribution has a high-contrast feature not seen in the experimental data. Both theoretical distributions have a prominent depression in density at ~12 nm from the outside edge of the distribution (corresponding to the inner edge of the nucleosome core), which is not seen in the experimental distributions of either tissue. Differences are expected, however, because histone H1 was not included in the computer-generated models. The radial density distributions of the hollow-solenoid models have large central holes that have full width at half maximum diameters of 18.1 and 11.9 nm for *Thyone* and *Necturus*, respectively. Thus, the solenoid models predict radial density distributions substantially different than the experimental data for both tissues.

Radii of gyration calculated from the empirically determined TMV, *Thyone*, and *Necturus* distributions were 6.4 nm (SD = 0.2 nm), 13.6 nm (SD = 0.9 nm), and 11.1 nm (SD = 1.3 nm), respectively. The SDs reflect the greater heterogeneity of the chromatin fibers than that of the TMV particles. Radii of gyration calculated from the radial density distributions of the computer-generated crossed-linker models were 13.6 nm for *Thyone* and 11.1 nm for *Necturus*. Values of 14.8 nm and 11.7 nm were obtained from the corresponding hollow-solenoid models.

Radiation Damage

Steven and co-workers (26) have shown that electron dose is an important variable in the determination of the radial density distribution. They determined that a radiation dose greater than 10^3 e^-/nm^2 disrupted the internal structure of frozen-dried TMV. With this consideration in mind, we divided the images into three groups: those receiving 100–200 e^-/nm^2; those receiving 200–400 e^-/nm^2; and those receiving 400–1,200 e^-/nm^2. Radial density distributions of TMV and *Thyone* fibers were calculated for each of these ranges, and no significant electron dose–dependent degradation of internal structure was observed.

Discussion

Quantitative EM is the most direct method to distinguish among the three classes of helical models for the chromatin fiber. Nevertheless, only one previous EM study has quantitatively compared the distribution of outer diameters of chromatin with different DNA linker lengths (37). That study, however, was subject to the potential artifacts of negative staining. Furthermore, the radial density distribution of stained chromatin cannot be determined. This study of unstained, frozen-dried fibers addresses these deficiencies. The resulting data do not support the solenoid or twisted-ribbon models, but are consistent with the double-helical crossed-linker models.

Radius of Gyration

Comparison of Radius of Gyration with Solution Studies. Calculation of the cross-sectional radius of gyration does not give direct information about the internal structure of the condensed chromatin fibers, but can test whether our limited sample of straight, frozen-dried fibers is representative of bulk chromatin. We have calculated the cross-sectional radius of gyration from the radial density distributions of *Thyone* (n = 87 bp) and *Necturus* (n = 48 bp) chromatin. Our values of 13.6 nm (SD = 0.9 nm) for *Thyone* and 11.1 nm (SD = 1.3 nm) for *Necturus* indicate a relationship between DNA linker length and the cross-sectional radius of gyration. These results are in support of the fiber diameter data reported by Williams et al. (37) and that of this study. Cross-sectional radii of gyration calculated from neutron scattering from chicken erythrocyte chromatin (R_c = 12.5 nm; n = 64 bp) and calf thymus chromatin (R_c = 11.3 nm; n = 45 bp) also suggest a correlation between DNA linker length and radius of gyration (9, 13). Comparison of our calculated cross-sectional radii of gyration with those obtained from x-ray solution scattering (Williams, S. P., and J. P. Langmore, manuscript in preparation) indicates that the fibers chosen for STEM analysis were apparently smaller than those present in bulk solution by 0, 14, and 2% for TMV, *Thyone*, and

Necturus, respectively. Thus, the thicker *Thyone* fibers were either undersampled, or had shrunken during dehydration. Spread-flattening of the fibers has been ruled out.

Diameter

Evidence that Chromatin Fiber Diameter Varies with DNA Linker Length. There has been considerable controversy regarding the diameter of the condensed chromatin fiber. Advocates of the solenoid and twisted-ribbon models of chromatin structure maintain that the diameter of the condensed chromatin fiber is 30 nm, independent of DNA linker length (10, 32, 33). In contrast, Williams et al. (37) and others (14, 15) have presented data suggesting that fiber diameter varies with DNA linker length, an explicit prediction of the crossed-linker models. We have presented STEM diameter measurements of chromatin fibers derived from two different tissues, with DNA linker lengths of 87 (*Thyone*) and 48 bp (*Necturus*). Our values of 38.0 nm (SD = 3.7 nm) for *Thyone* and 31.2 nm (SD = 3.6 nm) for *Necturus* indicate that fiber diameters are larger for chromatin with longer DNA linker length. These data are in excellent agreement with measurements made by Williams et al. (37) of *Thyone* and *Necturus* diameters using curve fitting to x-ray patterns from cell nuclei (39.4 nm for *Thyone* and 31.2 nm for *Necturus*) and transmission EM of fibers in negative stain (37.8 nm, SD = 3.8 nm; and 30.0 nm, SD = 3.1 nm).

Compatibility with Other Measurements. Other types of measurements have also indicated a relationship between fiber diameter and DNA linker length. Zentgraf and Franke (40) used EM to study the sizes of negatively stained chromatin particles ("super beads") from sea urchin sperm (n = 94 bp; mean particle size, 48 nm), chicken erythrocytes (n = 64 bp; mean particle size, 36 nm), and chicken and rat liver (n = 54 bp; mean particle size, 32 nm). They attributed the particle size differences to the state of cell differentiation. We interpret their samples to be short fragments of chromatin fibers having diameters dependent upon DNA linker length.

There is also evidence of differences between sea urchin chromatin and rat liver chromatin in solution. Thomas et al. (31) found a 30% greater sedimentation velocity for sea urchin sperm oligonucleosomes (n = 94 bp) than for rat liver oligonucleosomes (n = 54 bp) of the same molecular weight. Thomas et al. interpreted their results in terms of different flexibilities for fibers of constant diameter. Because the sedimentation velocity is much more sensitive to fiber length than diameter, we attribute their findings to the fact that sea urchin oligonucleosomes are shorter than rat liver oligonucleosomes of the same molecular weight. This interpretation is consistent with the crossed-linker models, which predict more nucleosomes per unit length for chromatin with longer DNA linker lengths (e.g., Fig. 2, *b* and *d*).

Our data and the data cited above do not agree with several studies which report constant fiber diameters, independent of DNA linker length. Widom et al. (35) reported similar diameters (~30 nm) for sea urchin sperm chromatin (n = 94 bp) and chicken erythrocyte chromatin (n = 64 bp). Their results were based on visual inspection of electron micrographs of unfixed, negatively stained fibers. Histograms of fiber diameters and statistical results were not given. McGhee et al. (20) also have reported constant fiber diameters, independent of DNA linker length. Their conclusions were based on the decay of linear dichroism signals from field-oriented chromatin fibers. The disagreement of their data with other dichroism data (7, 14, 23), however, suggests that their chromatin might have been distorted by the high electric field.

Comparison of Fiber Diameter with Predictions of the Crossed-Linker Models. There is a noticeable difference between fiber diameters determined by STEM and those calculated from the computer-generated crossed-linker models. The measured outer diameters of *Thyone* and *Necturus* chromatin were 38.0 and 31.2 nm, respectively. Measurements of computer-generated crossed-linker models built with the experimental values for the average DNA linker lengths gave outer diameters of 41.9 and 28.3 nm for *Thyone* and *Necturus*, respectively (Fig. 3).

Diameter values derived by microscopy are subject to potential systematic errors such as: (*a*) shrinkage due to fixation or dehydration, possibly caused by a transition from B-form to A-form DNA; (*b*) flattening due to surface interactions; and (*c*) systematic selection of fibers with linker lengths that are not representative of bulk chromatin. Diameter values derived through model building also are subject to uncertainties. The computer-generated crossed-linker models for *Thyone* and *Necturus* chromatin contained straight linker DNA and thus have the maximum possible diameter. Alternative, curved paths for the linker DNA gave rise to smaller diameters without changing the helical parameters. Fortunately, direct determinations of fiber diameters in the frozen-hydrated state are in close agreement with the diameters of the crossed-linker models built with straight linkers (Athey, B. D., M. F. Smith, D. A. Rankert, S. P. Williams, and J. P. Langmore, manuscript in preparation). In addition, x-ray measurements of the cross-sectional radii of gyration of chromatin agree well with those determined from the computer models (Williams, S. P., and J. P. Langmore, manuscript in preparation). Thus, it is likely that the *Thyone* fibers have shrunken during STEM preparation.

Heterogeneity of Chromatin Fibers. The error analysis of our diameter data highlights one of the difficulties of chromatin structural studies. The SDs of the chromatin measurements were about six times higher than those of the TMV measurements. Also, the SD in the chromatin data was ~9% of the mean, whereas the SD in the TMV data was only 3% of the mean. The greater spread in the chromatin data might have been caused by: (*a*) inherent disorder or heterogeneity in the fibers, perhaps correlated with a variation in the length of linker DNA; or (*b*) greater distortion of chromatin during adsorption and dehydration onto the carbon film.

Evidence against Fiber Aggregation. Widom and Klug (34) have argued that the 40-nm chicken erythrocyte chromatin fibers found by Woodcock et al. (38) were due to side-by-side aggregation or interdigitation of 30-nm fibers. Their interpretation was based on visual inspection of their own electron micrographs, which exhibited aggregated fibers. Widom et al. (35) also have reported that fixation of sea urchin chromatin at very low ionic strength caused severe aggregation. Unfortunately, we have been unable to solubilize sea urchin sperm chromatin by our techniques. However, our data on fixed *Thyone* and *Necturus* chromatin were obtained from straight fibers, free of the aggregation and bifurcation seen in the micrographs of Widom et al. The histograms shown in Fig. 5 do not show evidence of a bimodal

distribution, which might be expected in the presence of limited aggregation.

Calculated radial density distributions of frozen-hydrated *Thyone* and *Necturus* chromatin in buffer EB exhibited high density at all radii and featured clearly defined nucleosome peaks which differed only in radial position (Smith, M. F., et al., manuscript in preparation). These results are consistent with a conserved packing of nucleosomes at the periphery of the fiber. It would be difficult to explain how unaggregated and aggregated fibers would give the same detailed density distribution at the fiber edge. Diameter measurements of frozen-hydrated chromatin isolated at lower salt concentration (0.8 mM $MgCl_2$), and prepared under mild fixation conditions (0.1% glutaraldehyde for 5 h) gave diameters that were in quantitative agreement with those obtained from extensively fixed chromatin in buffer EB (Smith, M. F., B. D. Athey, D. A. Rankert, S. P. Williams, and J. P. Langmore, in preparation). These results suggest that the fiber structure is insensitive to certain changes in salt and fixation, both variables that might influence the degree of aggregation.

Aggregation of chromatin in EB has not been seen by low-angle x-ray scattering of *Thyone*, *Necturus*, and chicken chromatin at several different chromatin concentrations (Williams, S. P., and J. P. Langmore, in preparation). Both the radius of gyration and the mass per unit length showed a strong correlation with DNA linker length, which was completely independent of the chromatin concentration and in quantitative agreement with the results of this paper. Fixation studies of cell nuclei and isolated fibers revealed only slight changes in external fiber geometry during fixation. All these data demonstrate that the differences in chromatin fiber morphology reported here and by others are not due to fiber aggregation.

Distribution of Radial Density

Calculation of the radial distribution of density from electron micrographs of unstained samples is the most direct method available to test whether fibrous biological molecules have solid or hollow centers. Furthermore, STEM distributions can be directly compared to those obtained from computer-generated models or those obtained from other experimental techniques. Using this approach, it was possible to test: (*a*) whether our TMV radial density results were consistent with those obtained by others and (*b*) whether the radial density distributions of chromatin were consistent with the predictions of particular models for chromatin fiber structure.

Visualization of the Central Hole in TMV. x-ray fiber diffraction has established that TMV have three regions of high density at approximate radii of 2.7, 4.0, and 6.8 nm, and a central hole of ~2 nm radius (12, 21). Our EM, and that of others (26) reveal density peaks at around 2.7, 5.0, and 6.8 nm radius, and a central hole. The peaks at 2.7 and 6.8 nm radius most likely correspond to a series of reverse turns (formerly called V helices), and several short regions of β-sheet (21). The strong density peak at 4.0 nm radius found by x-ray fiber diffraction corresponds to the viral RNA, which scatters more strongly in solution than protein. However, in vacuum, protein and nucleic acid have very similar scattering properties. Therefore, the viral RNA peak is not visible in the STEM radial density distributions. The peak at ~5.0 nm radius found here and by Steven et al. (26) most likely corresponds to the four alpha helices (LS, RS, LL, LR) described by Namba et al. (21). Radial density distributions of RNA-free TMV coat protein polymers also exhibit a peak at ~5.0 nm radius by both techniques (12, 26). STEM can reveal the position of the RNA, however, by taking the difference between the radial densities of TMV virions and TMV coat protein polymers (26).

Closer comparison of the results of Steven et al. (26) and those of the present study reveals two slight differences. Steven et al. found that the 2.7- and 5.0-nm radius peaks have almost the same density. They also found a larger depression in density at the center of the distributions. Their analysis included only those few TMV particles that upon visual inspection gave an indication of a central hole. Our analysis also included those TMV particles that did not show evidence of central holes by visual inspection. The radial reconstruction of the randomly chosen TMV molecules still revealed the three density peaks and the central hole. Therefore, it is significant that the radial reconstructions from randomly chosen chromatin fibers did not reveal a central hole.

Evidence that Chromatin Fibers Have Solid Centers. One of the major structural differences of the proposed chromatin models is the presence or absence of a central hole. Until now, however, this question had not been addressed directly. Data in support of solid fibers had either come from indirect techniques (e.g., neutron scattering) or from techniques which often lead to ambiguous interpretations (e.g., microscopy of stained and embedded nuclei). Our STEM analysis is the first study to directly determine the radial density distribution of chromatin. These data from unstained samples clearly show high density at the center of chromatin fibers (Fig. 8).

Suau et al. (28) and Dunn et al. (9) also have suggested that chromatin fibers are solid. Their results were obtained indirectly by curve fitting the calculated distance distribution functions from neutron scattering patterns of chicken erythrocyte chromatin (n = 64 bp). They suggested that the data were best fit by rod-like models with solid centers and a maximum diameter of 34 nm. To explain the data, Suau et al. proposed a solenoid model with every seventh nucleosome at the center of the fiber. Dunn, on the other hand, concluded that a solenoid with the center filled with linker DNA and histone H1 best represented the data. These neutron data are in support of our radial density measurements.

Earlier EM data had given ambiguous information about the centers of chromatin fibers. Davies et al. (6) found stain at the center of chromatin fibers in thin sections of embedded chicken erythrocyte nuclei. They interpreted these findings as positive staining of a DNA-rich center. Finch and Klug (11), however, suggested that those highly-stained regions were due to accumulation of negative or positive stain in a hollow center. Subirana and co-workers (29) also studied chromatin in thin sections of embedded nuclei. They calculated a three-dimensional reconstruction of dehydrated, embedded, and stained chromatin from *Holothuria tubulosa* sperm (n = 81 bp) at low salt (0.4 mM $CaCl_2$). Their results indicated a non-helical fiber with a diameter of 28 nm and no central hole. They proposed a "layered-zigzag" model with five to six nucleosomes per layer and linker DNA structurally incorporated onto the nucleosome core. Langmore and Paulson (17) questioned the validity of these and other studies of embedded chromatin. They showed that dehydra-

tion and embedding of chromatin caused complete loss of the x-ray peaks that are characteristic of chromatin structure as well as shrinkage of the distance between chromatin fibers. These deleterious effects could explain the small fiber diameter, low mass per unit length, and nonhelical structure reported by Subirana et al. Our view is that, regardless of the obvious problem of specimen preservation in thin sections, the uncertainty in the relative amounts of negative or positive staining make it impossible to interpret the low-resolution images of plastic-embedded chromatin. The contradictory conclusions of Davies, Finch, and Subirana reinforce this view.

Comparison with Computer Models. Radial density distributions of computer-generated crossed-linker and hollow-solenoid models were calculated and compared with our STEM radial density data. Although analysis of this sort can not unambiguously prove whether a particular model is correct, it can be used to evaluate the plausibility of a particular model and pinpoint specific inconsistencies with the data.

We have calculated radial density distributions of the double-helical crossed-linker models described by Williams et al. (37). The slight internal variation in density found in the *Necturus* model distribution, but not found in the data, is conceivably due to the absence of histone H1 in the computer-generated models. H1, which comprises ~10% of the chromatin fiber mass, would fill open volume in the model, possibly reducing the internal density variations. The large difference between the empirical and model distributions of *Thyone* chromatin appears to be localized to the position of the linker DNA. This is possibly due to the difficulty in modeling the apparent shrinkage of the *Thyone* fibers in the STEM. To build the *Thyone* model with a diameter of 38 nm, a straight linker with 0.28 nm per basepair was used. Perhaps by coincidence, partially dehydrated DNA is known to have a rise of ~0.25 nm per basepair (36). Another possible model would have the correct length of DNA bent in a plane perpendicular to the long axis of the fiber, thus shifting some of the linker DNA scattering away from the center. This type of model gives better agreement with the *Thyone* data (results not shown).

Radial density distributions were calculated from hollow-solenoid models built with mean outer diameters equal to those measured for *Thyone* and *Necturus* chromatin. The models were intentionally smeared to take into account the uncertainties in the fiber diameter analysis. Subsequent radial density distributions exhibited central holes of 18.1 and 11.9 nm diameter, respectively (Fig. 8). Thus, even when we modeled the uncertainties of the STEM analysis, the solenoids still showed significant central holes. The hollow-twisted-ribbon model proposed by Woodcock et al. (38) would give radial density distributions very similar to those of the hollow-solenoid. Because our TMV results were sensitive enough to reveal a hole of 2–4 nm in diameter, it is significant that we did not detect even a small depression at the center of the chromatin distributions.

Could H1, which is absent in the computer-generated models, account for enough mass to fill in the central holes in the hollow-solenoid and hollow-twisted-ribbon models? H1 consists of a conserved globular domain and two highly basic termini. Most likely the basic tails are closely associated with DNA. Thus, only the globular domain would be free to occupy the center of the "hollow" models. The globular domain is estimated to be more or less spherical, with a diameter of only 2.9 nm (1), and a molecular weight that represents <5% of chromatin. Therefore, H1 is too small to occupy a significant part of the predicted 18.1- and 11.9-nm holes in the smoothed models, which compose ~22 and 14% of the total volume. Thus, the existence of high density at the center of chromatin fibers is inconsistent with the hollow-solenoid and hollow-twisted-ribbon models.

Predictions of Other Models. There are three models in addition to the double-helical crossed-linker models that have solid centers. These are the solid-solenoid model of Butler (5), the twisted-ribbon model of Worcel et al. (39), and the triple-helical crossed-linker model of Makarov et al. (19). Butler maintains that the diameter of the solid-solenoid is independent of DNA linker length, although this constraint is not inherent in the structure. A diameter dependence upon DNA linker length is difficult to envision in this model, but can not be ruled out. The Worcel model predicts a slight diameter dependence upon DNA linker length, but not enough to account for the differences found in this and other studies. The Makarov model predicts diameters in agreement with our measurements, but is inconsistent with the spacing and orientation of the diffraction features obtained from partially oriented chromatin (34) and individual fibers (37).

In addition to the double-helical and triple-helical crossed-linker models, two other crossed-linker models have been proposed: the one- (24) and five-gyre (4) models. These models predict outer diameters for chicken erythrocyte chromatin (n = 64 bp) that are 10 to 15% larger than estimates obtained by x-ray scattering (14, 37, Williams, S. P., and J. P. Langmore, manuscript in preparation) or predicted by the double-helical models (37). Furthermore, we estimate that these models have large central holes of ~12% of the outer diameter. The paths of the linker DNA would have to be extensively modified for these models to fit the diameter and radial density data.

Summary. There has been limited progress in the collection of high-resolution data on the three-dimensional structure of chromatin. Nevertheless, we have been able to use the low-resolution electron images to establish that isolated chromatin fibers have: (*a*) significant heterogeneity of fiber diameter; (*b*) larger fiber diameters for chromatin with longer DNA linker length; and (*c*) relatively uniform density at all radii, with no evidence of a central hole. Until higher resolution data is obtained, we can only attempt to fit low-resolution data to proposed models. Using this approach, we have shown that the only existing models for chromatin structure that are consistent with the data are the double-helical crossed-linker models. Further tests of this proposed structure will require higher resolution data.

We would like to thank D. Rankert for help in manuscript preparation; J. Hainfeld, P. Kito, K. Chung, K. Monson, and J. Wall for aid with the microscopy; and A. Steven, P. Furcinitti, and J. Wall for provision of the radial density programs.

These studies were supported by National Institutes of Health (NIH) grant GM27937 and National Science Foundation DIR-8706052 to J. P. Langmore; the Brookhaven STEM was supported by NIH grant RR-01777 and the Department of Energy; B. D. Athey was supported by predoctoral training grant T32 GM-07315.

Received for publication 19 June 1989 and in revised form 4 October 1989.

References

1. Allen, J., P. G. Hartman, C. Crane-Robinson, and F. X. Aviles. 1980. The structure of histone H1 and its location in chromatin. *Nature (Lond.).* 288:675–679.
2. Baldwin, J. P. 1986. Chromatin structure studies using neutron beams. *Physica.* 138B:236–240.
3. Bordas, J., L. Perez-Grau, M. H. J. Koch, M. C. Vega, and C. Nave. 1986. The superstructure of chromatin and its condensation mechanism. I. Synchrotron radiation x-ray scattering results. *Eur. Biophys. J.* 13:157–173.
4. Bordas, J., L. Perez-Grau, M. H. J. Koch, M. C. Vega, and C. Nave. 1986. The superstructure of chromatin and its condensation mechanism. II. Theoretical analysis of the x-ray scattering patterns and model calculations. *Eur. Biophys. J.* 13:175–185.
5. Butler, P. J. G. 1984. A defined structure of the 30 nm chromatin fibre which accommodates different nucleosomal repeat lengths. *EMBO (Eur. Mol. Biol. Organ.) J.* 3:2599–2604.
6. Davies, H. G., A. B. Murray, and M. E. Walmsley. 1974. Electron-microscope observations on the organization of the nucleus in chicken erythrocytes and a superunit thread hypothesis for chromatin structure. *J. Cell Sci.* 16:261–299.
7. Dimitrov, S. I., I. V. Smirnov, and V. L. Makarov. 1988. Optical anisotropy of chromatin. Flow linear dichroism and electric dichroism studies. *J. Biomol. Struct. Dyn.* 2:1135–1148.
8. Duda, R. L., J. S. Wall, J. F. Hainfeld, R. M. Sweet, and F. A. Eiserling. 1985. Mass distribution of a probable tail-length-determining protein in bacteriophage T4. *Proc. Natl. Acad. Sci. USA.* 82:5550–5554.
9. Dunn, S. P., J. P. Baldwin, L. Wyns, S. Muyldermans, I. Lasters, G. A. Poland, D. Z. Staynov, H. W. E. Rattle, and M. J. Wood. 1986. Neutron scattering of chromatin multinucleosomes. *Physica.* 136B:265–267.
10. Felsenfeld, G., and J. D. McGhee. 1986. Structure of the 30 nm chromatin fiber. *Cell.* 44:375–377.
11. Finch, J. T., and A. Klug. 1976. Solenoid model for superstructure in chromatin. *Proc. Natl. Acad. Sci. USA.* 73:1897–1901.
12. Franklin, R. E., and K. C. Holmes. 1958. Tobacco Mosaic Virus: Application of the method of isomorphous replacement to the determination of the helical parameters and radial density distribution. *Acta. Crystallogr. Sect. B. Struct. Crystallogr. Cryst. Chem.* 11:213–220.
13. Gerchman, S. E., and V. Ramakrishnan. 1987. Chromatin higher-order structure studied by neutron scattering and scanning transmission electron microscopy. *Proc. Natl. Acad. Sci. USA.* 84:7802–7806.
14. Koch, M. H. J., Z. Sayers, A. M. Michon, R. Marquet, C. Houssier, and J. Willfuhr. 1988. The superstructure of chromatin and its condensation mechanism. V: Effect of linker length, condensation by multivalent cations, solubility and electric dichroism properties. *Eur. Biophys. J.* 16:177–185.
15. Koch, M. H. J., M. C. Vega, Z. Sayers, and A. M. Michon. 1987. The superstructure of chromatin and its condensation mechanism. III: Effect of monovalent and divalent cations x-ray solution scattering and hydrodynamic studies. *Eur. Biophys. J.* 14:307–319.
16. Lamvik, M. K., and J. P. Langmore. 1977. Determination of particle mass using scanning transmission electron microscopy. *In* Scanning Electron Microscopy/1977. Vol. 1.O. Johari, editor. IIT Research Institute, Chicago, IL. 401–409.
17. Langmore, J. P., and J. R. Paulson. 1983. Low angle x-ray diffraction studies of chromatin structure in vivo and in isolated nuclei and metaphase chromosomes. *J. Cell Biol.* 96:1120–1131.
18. Langmore, J. P., J. Wall, and M. S. Isaacson. 1973. The collection of scattered electrons in dark field electron microscopy I. Elastic scattering. *Optik.* 38:335–350.
19. Makarov, V., S. Dimitrov, V. Smirnov, and I. Pashev. 1985. A triple helix model for the structure of chromatin fiber. *FEBS (Fed. Eur. Biochem. Soc.) Lett.* 181:357–361.
20. McGhee, J. D., J. M. Nickol, G. Felsenfeld, and D. C. Rao. 1983. Higher order structure of chromatin: orientation of nucleosomes within the 30 nm chromatin solenoid is independent of species and spacer length. *Cell.* 33:831–841.
21. Namba, K., R. Pattanayek, and G. Stubbs. 1989. Visualization of protein-nucleic acid interactions in a virus: refined structure of intact Tobacco Mosaic Virus at 2.9 Å resolution by x-ray fiber diffraction. *J. Mol. Biol.* 208:307–325.
22. Richmond, T. J., J. T. Finch, B. Rushton, D. Rhodes, and A. Klug. 1984. Structure of the nucleosome core particle at 7 Å resolution. *Nature (Lond.).* 311:532–537.
23. Sen, D., S. Mitra, and D. M. Crothers. 1986. Higher order structure of chromatin: evidence from photochemically detected linear dichroism. *Biochemistry.* 25:3441–3447.
24. Staynov, D. Z. 1983. Possible nucleosome arrangements in the higher-order structure of chromatin. *Int. J. Biol. Macromol.* 5:3–10.
25. Steven, A. C., M. E. Bisher, B. L. Trus, D. Thomas, J. M. Zhang, and J. L. Cowell. 1986. Helical structure of *Bordetella pertussis* fimbriae. *J. Bacteriol.* 167:968–974.
26. Steven, A. C., J. F. Hainfeld, B. L. Trus, P. M. Steinert, and J. S. Wall. 1984. Radial distributions of density within macromolecular complexes determined from dark-field electron micrographs. *Proc. Natl. Acad. Sci. USA.* 81:6363–6367.
27. Steven, A. C., T. A. Simpson, B. L. Trus, P. S. Furcinitti, J. F. Hainfeld, and J. S. Wall. 1986. Radial density profiles of macromolecular filaments determined from dark-field scanning transmission electron micrographs: improvements in technique and some applications. *Ann. NY Acad. Sci.* 483:188–198.
28. Suau, P., E. M. Bradbury, and J. P. Baldwin. 1979. Higher-order structures of chromatin in solution. *Eur. J. Biochem.* 97:593–602.
29. Subirana, J. A., S. Munoz-Guerra, J. Aymami, M. Radermacher, and J. Frank. 1985. The layered organization of nucleosomes in 30 nm chromatin fibers. *Chromosoma (Berl.).* 91:377–390.
30. Thoma, F., Th. Koller, and A. Klug. 1979. Involvement of histone H1 in the organization of the nucleosome and of the salt-dependent superstructure of chromatin. *J. Cell Biol.* 83:403–427.
31. Thomas, J. O., C. Rees, and P. J. G. Butler. 1986. Salt-induced folding of sea urchin sperm chromatin. *Eur. J. Biochem.* 154:343–348.
32. van Holde, K. E. 1989. Chromatin. Springer-Verlag, New York. 219–355.
33. Widom, J. 1989. Toward a unified model of chromatin folding. *Annu. Rev. Biophys. Chem.* 18:365–395.
34. Widom, J., and A. Klug. 1985. Structure of the 300Å chromatin filament: x-ray diffraction from oriented samples. *Cell.* 43:207–213.
35. Widom, J., J. T. Finch, and J. O. Thomas. 1986. Higher-order structure of long repeat chromatin. *EMBO (Eur. Mol. Biol. Organ.) J.* 4:3189–3194.
36. Wilkins, M. H. F. 1963. Molecular configuration of nucleic acids. *Science (Wash. DC).* 140:941–950.
37. Williams, S. P., B. D. Athey, L. J. Muglia, R. S. Schappe, A. H. Gough, and J. P. Langmore. 1986. Chromatin fibers are left-handed double helices with diameters and mass per unit length that depend on linker length. *Biophys. J.* 49:233–248.
38. Woodcock, C. L. F., L.-L. Y. Frado, and J. B. Rattner. 1984. The higher-order structure of chromatin: evidence for a helical ribbon arrangement. *J. Cell Biol.* 99:42–52.
39. Worcel, A., S. Strogatz, and D. Riley. 1981. Structure of chromatin and the linking number of DNA. *Proc. Natl. Acad. Sci. USA.* 78:1461–1465.
40. Zentgraf, H., and W. W. Franke. 1984. Differences of supranucleosomal organization in different kinds of chromatin: cell type-specific globular subunits containing different numbers of nucleosomes. *J. Cell Biol.* 99:272–286.